JOURNAL OF CATALYSIS 149, 375–389 (1994)

Investigation of the Mechanism of Ammonia Oxidation and Oxygen Exchange over Vanadia Catalysts Using N-15 and O-18 Tracer Studies[1]

Umit S. Ozkan,[2] Yeping Cai,[3] and Mahesh W. Kumthekar

Department of Chemical Engineering, The Ohio State University, Columbus, Ohio 43210

Received October 19, 1993; accepted June 13, 1993

Isotopic labeling studies in ammonia oxidation and oxygen exchange have been performed over unsupported vanadia catalysts having preferential exposure of different crystal planes. All catalysts were characterized using BET surface area measurement, X-ray diffraction, laser Raman spectroscopy, X-ray photoelectron spectroscopy, scanning electron microscopy, 3-D imaging, and temperature-programmed adsorption/desorption/reduction techniques. Isotopic labeling studies have been performed under steady-state conditions by using $^{16}O_2 \rightarrow {}^{18}O_2$, $NH_3 + {}^{16}O_2 \rightarrow NH_3 + {}^{18}O_2$, and $^{14}NH_3 + O_2 \rightarrow {}^{15}NH_3 + O_2$ switches. The experimentally obtained transients have been compared to those calculated through a mathematical simulation. Results of the oxygen exchange experiments show that, although there is no formation of the cross-labeled oxygen, gaseous oxygen actively exchanges with lattice oxygen on all crystal planes of V_2O_5. The oxygen located on the (010) basal plane seems to be more reactive whereas the replenishment of oxygen from the catalyst bulk appears to be faster towards the side planes of the V_2O_5 crystals. The kinetic experiments performed for ammonia oxidation reaction studies suggest that there are at least two types of sites on the (010) plane responsible for this reaction, one leading to NO formation and the other one leading to N_2 and N_2O formation. The type of adsorbed ammonia species formed are thought to be controlled by the immediate environment of the V = O species on the surface.

INTRODUCTION

NO_x abatement from the effluents of stationary and mobile sources continues to be the focus of interest because of growing public concern and stricter regulations regarding air pollution control. Vanadia-based catalysts have proved to be quite effective for selective catalytic reduction (SCR) of nitric oxide with ammonia (1–9). Most of the work done in this area has recently been summarized in two review articles (10, 11). There have been several studies attempting to elucidate the mechanism of this reaction over vanadia-based catalysts (8, 12–19). Various characterization techniques, including LRS, FT-IR, XPS, and NMR, have been used to identify the surface species and the intermediates taking part in the SCR reactions. In spite of the widely accepted significance of the present SCR technology as a NO_x emission control technique and the large number of studies conducted over the commercial SCR catalysts, there still remain unresolved questions about the reaction network and selectivity control in these reactions.

One of the earlier mechanisms proposed for SCR reactions was that of Takagi *et al.* (12), who proposed a Langmuir–Hinshelwood mechanism for the SCR reaction producing N_2 and H_2O. An Eley–Rideal mechanism for the SCR reaction was proposed by Inomata *et al.* (13), who suggested that the reaction proceeded between strongly adsorbed NH_3 and gaseous NO and that the reduced surface V–OH species were reoxidized to V = O by either gaseous oxygen or bulk oxygen. Janssen *et al.* (8, 14, 15), who investigated the mechanism of the reaction of NO with NH_3 over vanadia catalysts by using isotopic transient techniques, proposed the V = O species to be the active sites for ammonia activation and suggested that the sites that were easily reduced had a higher activity. Gasior *et al.* (16) investigated the mechanism of the SCR reactions over unsupported vanadium pentoxide catalysts by pulse reaction technique and suggested that ammonia was adsorbed on Bronsted sites which were located on the side planes of vanadium pentoxide crystals and NO was either very weakly adsorbed or not adsorbed at all. Odriozola *et al.* (17) reported NH_3 adsorption to take place on both TiO_2 and V_2O_5 as well as on reduced V_2O_5 surfaces, while NO adsorption occurred only on TiO_2 and on reduced V_2O_5, but not on oxidized V_2O_5 surfaces. They

[1] Any opinions, findings, and conclusions or recommendations expressed in this publication are those of the authors and do not necessarily reflect the views of the EPA.

[2] To whom correspondence should be addressed. Fax: (614) 292-3769. E-mail: ozkan.1@osu.edu.

[3] Present address: Lehigh University, Department of Chemical Engineering, Bethlehem, PA 18015.

0021-9517/94 $6.00

linked the catalyst effectiveness in vanadia/titania system to NO adsorption on the support. Adsorption of NO_x and NH_3 on vanadia catalysts supported over titania was also studied by Ramis *et al.* (18) who reported the presence of nitrosyl and nitrate species on the surface detected by FT-IR. Recently, Went *et al.* (19–21) proposed monomeric vanadyl and polymeric vanadate species on the surface of V_2O_5/TiO_2 catalysts to be the active species in SCR reaction and correlated the activity and selectivity to the relative abundance of these species.

In our earlier studies, we examined the activity and selectivity of vanadia catalysts on both anatase and rutile phases of the titania support (22, 23). Our later work was focused on the unsupported vanadia catalysts and was aimed at investigating the structural specificity of vanadia catalysts in selective catalytic reduction of nitric oxide (24) and the role of ammonia oxidation reaction in the SCR system (25). These studies, which combined bulk characterization and kinetic studies with temperature-programmed techniques, demonstrated the existence of catalytic anisotropy in SCR and in ammonia oxidation reactions over V_2O_5 crystals and provided clues about the adsorption/desorption behavior of these catalysts. As part of our continuing effort to understand the mechanism of the SCR reactions over these catalysts, in this article, we report our findings from the isotopic labeling studies performed during steady-state ammonia oxidation reactions. The main objective has been to differentiate between possible reaction pathways, to determine the role of lattice and gas phase oxygen in the reaction and to examine the differences between the surface residence time of nitrogen containing species. The experimental data have been interpreted in terms of a mathematical simulation based on unsteady state mole balances written for gas phase and surface species. The results are discussed with regard to the role played by direct ammonia oxidation reactions in the overall SCR scheme and the oxygen exchange characteristics of vanadia catalysts. Results of isotopic labeling studies using oxygen-labeled and nitrogen-labeled reactants in SCR reactions are presented elsewhere (26).

EXPERIMENTAL

Catalyst Preparation

Thermal treatment techniques were used to grow vanadium pentoxide particles preferentially exposing different crystal planes, as described earlier (24). The two samples used in this study, denoted as V_2O_5-D and V_2O_5-M, were prepared by calcining ammonium metavanadate (NH_4VO_3) (Aldrich) at 520°C for 50 hours in a flow of oxygen and by melting pure V_2O_5 (99.6% pure, Aldrich) at 695°C for 2 h and then subjecting it to temperature-programmed cooling for recrystallization, respectively. Both samples were sieved for uniform particle size distribution and used in the reactor without pelletizing. The specific surface areas of V_2O_5-D and V_2O_5-M were 3.4 and 1.0 m^2/g, respectively.

Catalyst Characterization

The specific surface areas of the catalysts were measured using the BET technique with a Micromeritics 2100 E Accusorb instrument. Krypton was used as the adsorbate. X-ray powder diffraction patterns were obtained using a Scintag PAD V diffractometer. Cu$K\alpha$ radiation (λ = 1.5432 Å) was used as the incident X-ray source. The surface morphology of the catalysts was examined through a Hitachi S-510 scanning electron microscope using a voltage of 25 kV and magnifications ranging from 100× to 8000×. A 3-D imaging technique was used in combination with the SEM studies to quantify the surface dimensions of the particles. The catalyst samples were also characterized using two laser Raman spectrometers (SPEX 1403 Ramalog 9-I spectrometer and SPEX 1877 Triplemate Raman spectrometer) which used 5-W argon ion lasers (Spectra Physics, Model 2016 and Model 2017) as the excitation source. X-ray photoelectron spectra of the samples were obtained using a Physical Electronics/Perkin Elmer (Model 550) ESCA/Auger spectrometer, operated at 15 kV and 20 mA. The X-ray source was Mg$K\alpha$ radiation (1253.6 eV). The binding energy of C 1*s* (284.6 eV) was used as a reference in these measurements. Details of the characterization experiments have been presented elsewhere (24).

Reaction Studies

The system used for isotopic studies with the switch from $^{16}O_2$ to $^{18}O_2$ is shown in Fig. 1. All tubing was $\frac{1}{8}$" (ea. 3 mm) 304 stainless steel unless otherwise stated. The two oxygen streams were connected by a 4-port Valco valve to perform the abrupt switch between $^{16}O_2$ and $^{18}O_2$. The flow diagram shown in Fig. 1 can be easily modified to perform other types of isotopic switches. The distance between the 4-port valve and the reactor was kept as short as possible in order to minimize traveling time for the gas in the system.

The feed gases consisted of 0.53% NH_3 in He (Linde), 10% O_2 in He (Linde), 10% $^{18}O_2$ in He (99 at.% ^{18}O, ICON), 0.5% $^{15}NH_3$ in He (99 at.% ^{15}N, ICON), and pure He (Linde). Each gas flow rate was controlled by a mass flow controller (Tylan Model FC-280), and displayed on a 4-channel readout box (Tylan Model RO-28). The mass flow controllers were calibrated for the specific gases prior to experiments.

All feed gases were mixed in a single stream prior to being sent to the reactor (Fig. 1). The reactor, made from

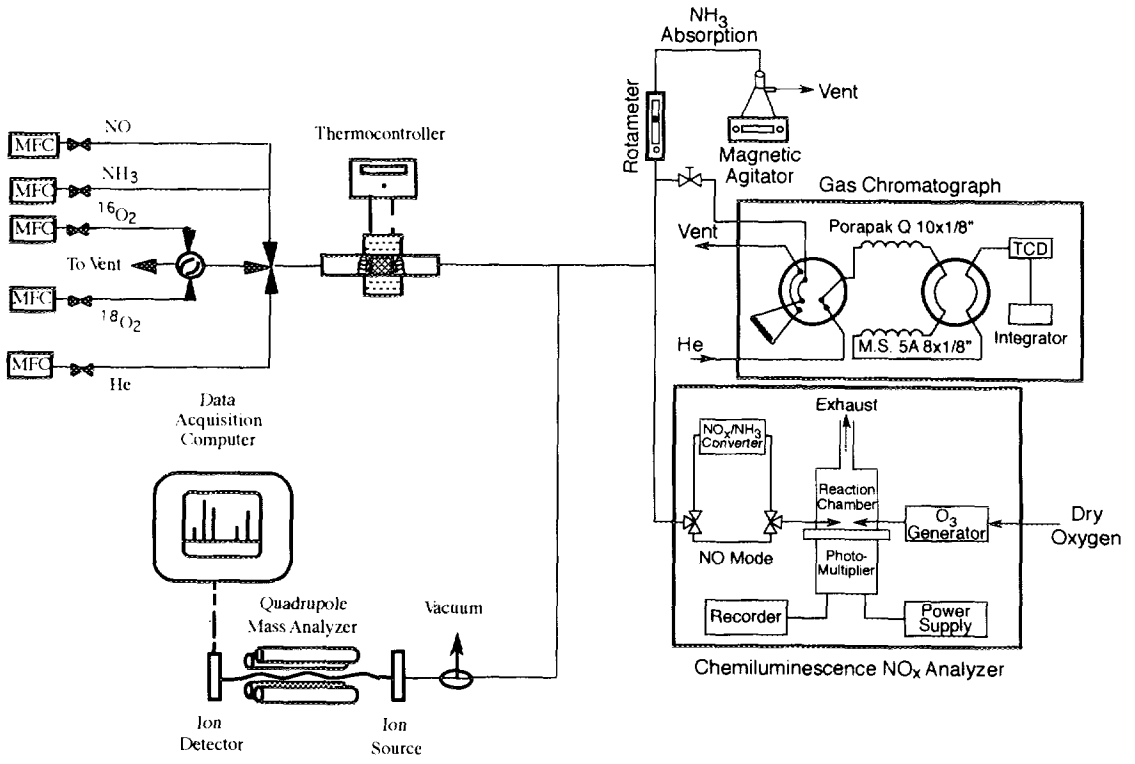

FIG. 1. Schematic of the experimental system used in isotopic labeling studies.

304 stainless steel tubing, measured 6.4 mm O.D. × 4.6 mm I.D., and 160 mm in length. The length of the catalyst bed varied from 5 to 10 mm. The catalyst loading was kept between 30 and 100 mg and was varied to achieve either equal total surface area or equal residence time in the reactor. Quartz wool was placed at both sides of the catalyst bed to fix the solids in place. The reactor was inserted into a stainless steel block for temperature control. Resistive heating cartridges (Watlow, C2A5) were used to heat the block. The temperature of the heating block was measured using a chromel–alumel type K thermocouple (Omega) and the temperature was controlled and displayed by a PID controller (Omega CN 9111). As found in previous experiments (22–25), the activity of the stainless steel tubing under reaction conditions was negligible.

The effluent gases from the reactor were analyzed by bleeding a small amount through a blank capillary column into a gas chromatograph–mass spectrometer (GC–MS) (Hewlett-Packard 5890 GC-Hewlett-Packard 5989A MS engine). The actual amount of effluent entering the MS detector was determined by the vacuum level inside the detector. The temperature in the MS source was kept at 100°C. The product analysis could also be carried through on-line gas chromatography and on-line chemiluminescence NO_x analyzer as described previously (23, 24). All the lines from the 4-port valve were heated up to 180°C in order to prevent any adsorption of reactant and product gases on the stainless steel tubing walls.

The isotopic labeling technique employed in the present study has been described in detail elsewhere (27, 28). The technique consists of allowing the reaction to reach steady-state using an unlabeled reaction mixture and abruptly switching from the unlabeled mixture to the labeled one. In doing so, the steady-state catalytic process is essentially unperturbed. Consequently, the total rate of formation of any product does not change due to the isotopic switch. By continuously monitoring the relaxation and evolution of the unlabeled and labeled species, isotopic transient curves can be obtained.

In this study, oxygen exchange and ammonia oxidation reactions have been examined using $^{16}O_2 \rightarrow {}^{18}O_2$, $NH_3 + {}^{16}O_2 \rightarrow {}^{15}NH_3 + {}^{18}O_2$ and $^{14}NH_3 + O_2 \rightarrow {}^{15}NH_3 + O_2$ switches over both V_2O_5-D and V_2O_5-M samples. In the oxygen exchange experiments, the concentrations of $^{16}O_2$ and $^{18}O_2$ were maintained at 0.89%, with He as the balance gas. In the ammonia oxidation reaction, the concentrations of ammonia and oxygen were kept at 1500 ppm and 0.89%, respectively, with helium as the balance gas. The reaction temperature was kept constant at 400°C. The reaction system was brought to steady-state, by keeping the reactor on line for at least 6 h before the isotopic

switch was made. The total volumetric flow rate through the reactor was maintained constant at 100 cm^3(STP)/min.

Data Analysis

Prior to performing the isotopic switches, fragmentation patterns were obtained for all reaction species, labeled as well as unlabeled, and the relative intensities were recorded for all fragments. These data were later used when correcting for interference from different fragments. All analyses were based on the assumption that the mass spectrometer response of each isotope for any given compound (e.g., ^{14}NO, ^{15}NO) was the same.

The transient for $^{14}NH_3$ was obtained by monitoring the signal for m/e = 16. The interference to the m/e = 16 signal from oxygen was corrected using the relative intensities of m/e = 16 and m/e = 32 signals for oxygen that were obtained independently under similar conditions. The transient for $^{15}NH_3$ was obtained by following the m/e = 17 signal. The interference from H_2O which has both m/e = 17 and m/e = 18 signals was corrected by using the relative intensity ratio of these two water fragments. A secondary correction was also used to account for the contribution to the m/e = 17 signal from $^{14}NH_3$ which was still in the system.

For all isotopes of N_2O, the molecular ion signals were used. The m/e signals followed were 44 or larger and they did not have any interference from any other species. $^{14}N^{16}O$, $^{15}N^{16}O$, $^{14}N^{18}O$, and $^{15}N^{18}O$ transients were obtained by following the m/e = 30, 31, 32, and 33 signals, respectively. The only correction needed was to the $^{14}N^{18}O$ signal (m/e = 32) for interference from oxygen. The nitrogen isotope transients were obtained by following m/e = 28, 29, and 30 signals. The m/e = 28 signal was used after the background correction. The $H_2{}^{16}O$ transients were obtained following the m/e = 18 signal. Corrections were made for interference from $^{15}NH_3$ or $^{18}O_2$ in those cases where the ammonia or oxygen were labeled. $H_2{}^{18}O$ transient was obtained using m/e = 20 signal. The oxygen isotopes $^{16}O_2$, $^{16}O^{18}O$, and $^{18}O_2$ transients were obtained by following the m/e = 32, 34, and 36 signals. The normalized concentration of each isotope for a given species was calculated by dividing the corrected signal for that isotope by the sum of the signals for all the isotopes of that species.

RESULTS

Catalyst Characterization

Characterization experiments which combined SEM, 3-D imaging, X-ray diffraction, X-ray photoelectron spectroscopy, and laser Raman spectroscopy techniques showed the preferential exposure of the (010) basal plane on V_2O_5-M and the side planes on V_2O_5-D. The scanning electron microscopy combined with 3-D imaging technique showed that V_2O_5-D consisted of thick and chunky crystals with the ratio of basal plane to side plane areas in the range of 1.5 to 1.9, while V_2O_5-M consisted of thin, long and sheet-like crystals with the same ratio in the range of 9.5 to 10.7, clearly indicating preferential exposure of the crystal planes. These observations were confirmed by XRD studies which showed a much higher relative intensity for diffraction bands resulting from (0k0) planes in V_2O_5-M. The Raman spectroscopy technique, on the other hand, showed a higher intensity of the band associated with V = O stretching vibration relative to the bands associated with bridging oxygen sites in the same sample. Details of these characterization results have been presented elsewhere (24).

Reaction Studies

Measurements for forcing function and mixing function. The isotopic labeling experiments are based on sending a step function change through the reactor that involves an abrupt switch from unlabeled reactant to a labeled reactant. The first set of experiments performed was intended to examine the response of the system for such a step change for an inert gas following the concepts presented earlier by Bennett and co-workers (29–32). The forcing function was measured by switching from Ar to O_2 in a completely empty reactor under conditions similar to the reaction conditions. The forcing function measurements showed the degree of deviation from an ideal step function due to back mixing in the transfer lines or in the empty reactor.

Mixing function measurements were done by sending a step function change, in our case a switch from Ar to oxygen, through the catalyst bed under reaction conditions. These measurements were repeated using different feed concentrations to check for reproducibility. Mixing function measurements represent the gas-phase hold up time or the mean residence time of an inert in the reactor and in the transfer lines. Figure 2 shows the experimental forcing function and mixing function curves. The mixing function measurements were performed over both catalyst beds. No major differences were observed in the time required for Ar to travel through the reactor system packed with V_2O_5-D or V_2O_5-M indicating no difference in the packing characteristics of the two catalyst beds.

$^{16}O_2 \rightarrow {}^{18}O_2$ Switch. The oxygen exchange transients in the absence of reactant gases over V_2O_5-D and V_2O_5-M within the first minute of the switch are plotted in Fig. 3. Also presented in this figure are the mixing function curves to provide direct comparison to the oxygen transients. The $^{16}O_2 \rightarrow {}^{18}O_2$ switch experiments were performed at 400°C at an oxygen concentration of 0.89% with He as the balance gas. No formation of cross-labeled

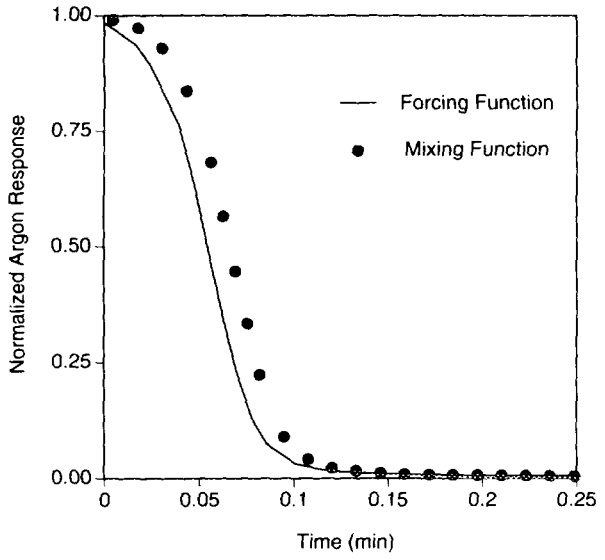

FIG. 2. Experimental forcing function and mixing function curves.

oxygen, i.e., $^{16}O^{18}O$, from the so-called scrambling process was observed over either sample. O_2 signals over V_2O_5-D or V_2O_5-M, however, did not decrease as rapidly as the inert signals did, indicating interaction with the surface. The O_2 signals remained at a steady value greater than zero for more than 10 min under the present experimental conditions indicating a steady participation of the lattice oxygen in the process.

A similar switching experiment performed in an empty reactor to examine homogeneous oxygen exchange and/or oxygen interaction with reactor walls showed immediate rise and decline of $^{18}O_2$ and $^{16}O_2$ signals respectively, with no cross-labeled oxygen being formed, eliminating the possibility of any homogeneous oxygen exchange under the reaction conditions used.

Although oxygen exchange transient curves were quite similar in shape over V_2O_5-D and V_2O_5-M, a significant difference in areas under the relaxation curves was observed in the experiments. This is a clear indication that the two samples have different ability in utilizing their lattice oxygen. V_2O_5-M was able to incorporate 194 μmol/m^2 ^{16}O into the gas phase over a 12-min period. V_2O_5-D, on the other hand, has only 113 μmol/m^2 of lattice ^{16}O incorporated into the gas phase over the same period.

$NH_3 + {}^{16}O_2 \rightarrow NH_3 + {}^{18}O_2$ Switch. Ammonia oxidation reactions were performed over both V_2O_5-D and V_2O_5-M catalysts by switching from unlabeled oxygen to labeled oxygen at steady state. These experiments were performed at 400°C with 1500 ppm ammonia and 0.89% oxygen in He. The transient curves of oxygen containing products, i.e. NO, N_2O, and H_2O, are presented in Figs. 4–6. The net rate of NO formation over V_2O_5-D was very low, which is in agreement with our earlier findings (25). Over V_2O_5-M, the nitric oxide formation was much more significant. For several minutes following the switch, there was still a significant amount of $N^{16}O$ present in the gas phase over this catalyst, produced from ammonia oxidation using the lattice oxygen. The $N^{16}O$ signal declined fairly rapidly and became zero seven minutes after the switch (Fig. 4). The nitrous oxide transient curves shown in Fig. 5 indicate that the unlabeled N_2O concentrations over V_2O_5-M declined rapidly and fell to zero approximately 8 min after the switch while it remained fairly high over V_2O_5-D. Unlabeled water concentrations (Fig. 6) did not reach zero within the time period studied over

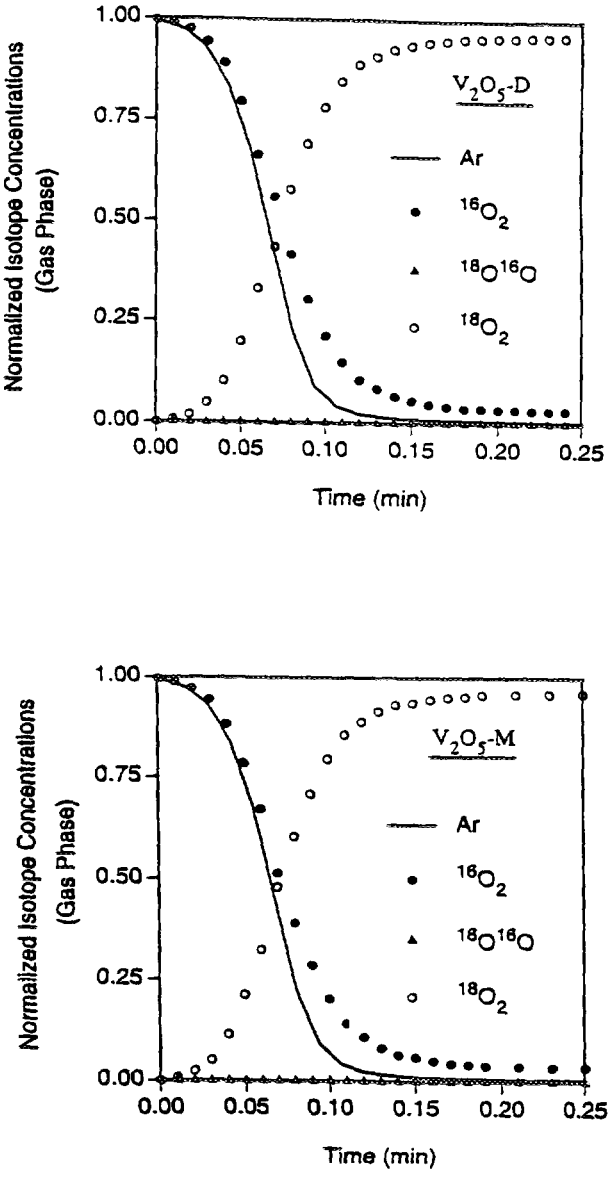

FIG. 3. Normalized oxygen isotope and argon concentrations in the absence of reactants.

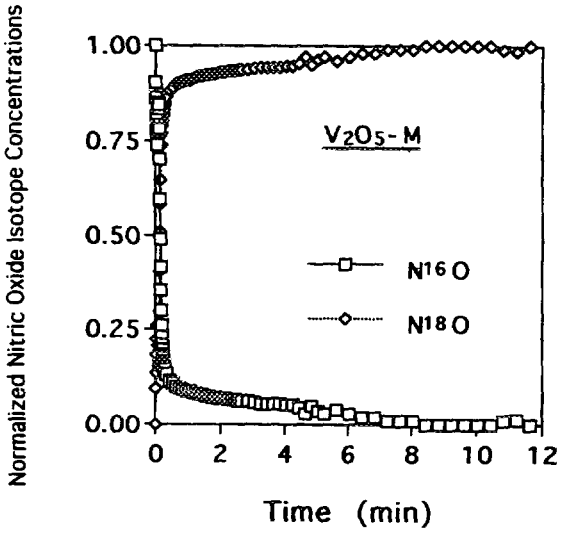

FIG. 4. Normalized nitric oxide isotope concentrations in the $NH_3 + O_2 \rightarrow NH_3 + {}^{18}O_2$ switch over V_2O_5-M.

either catalyst. However, the percentage of unlabeled oxygen incorporated into water over V_2O_5-D was considerably higher than it was over V_2O_5-M. Another interesting feature of these transients is the fact that the N_2O and

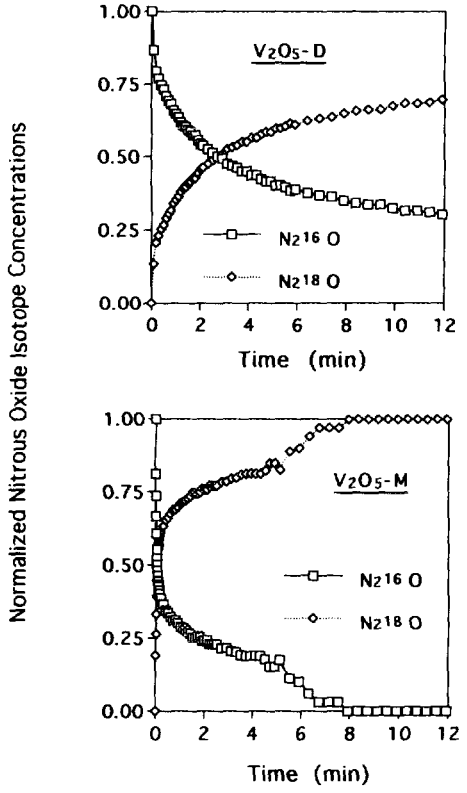

FIG. 5. Normalized nitrous oxide isotope concentrations in the $NH_3 + O_2 \rightarrow NH_3 + {}^{18}O_2$ switch.

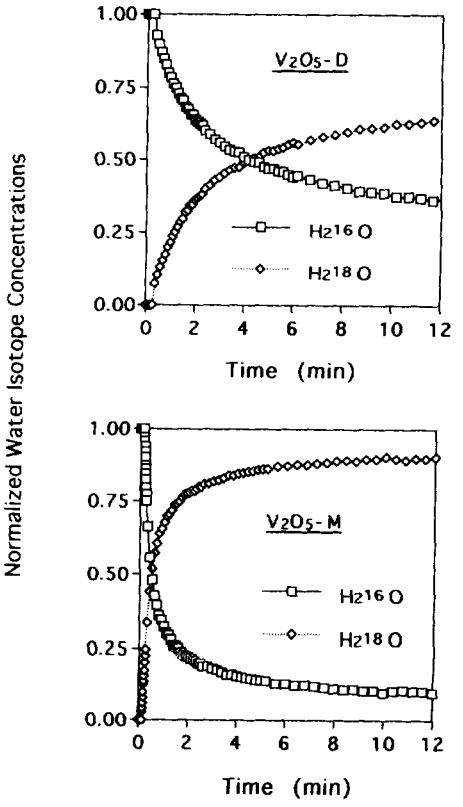

FIG. 6. Normalized water isotope concentrations in the $NH_3 + O_2 \rightarrow NH_3 + {}^{18}O_2$ switch.

H_2O transients were quite similar over the V_2O_5-D catalyst while it exhibited considerably different decline and rise behavior over V_2O_5-M.

A comparison of the ^{16}O incorporation rates for the two catalysts indicates that, 1 min after the switch, the total rate of ^{16}O incorporation into the products is higher over V_2O_5-M than it is over V_2O_5-D. However, by the end of the 12th min, there is more unlabeled oxygen being incorporated into products over V_2O_5-D than over V_2O_5-M.

Based on the total amount of water formed within the first 12 min after the switch, 52% was found to be water with unlabeled oxygen over V_2O_5-D and only 16% over V_2O_5-M. The corresponding values for nitric oxide and nitrous oxide were 19% and 46% over V_2O_5-D and 4% and 11% over V_2O_5-M, respectively.

$^{14}NH_3 + O_2 \rightarrow {}^{15}NH_3 + O_2$ switch. Ammonia oxidation reactions were also investigated over both V_2O_5-D and V_2O_5-M catalysts with the switch from $^{14}NH_3$ to $^{15}NH_3$. The concentration of inlet ammonia was maintained at 1500 ppm throughout the reaction. The oxygen concentration was maintained at 0.89%. The reaction was performed at 400°C. The observed formation rate of nitric

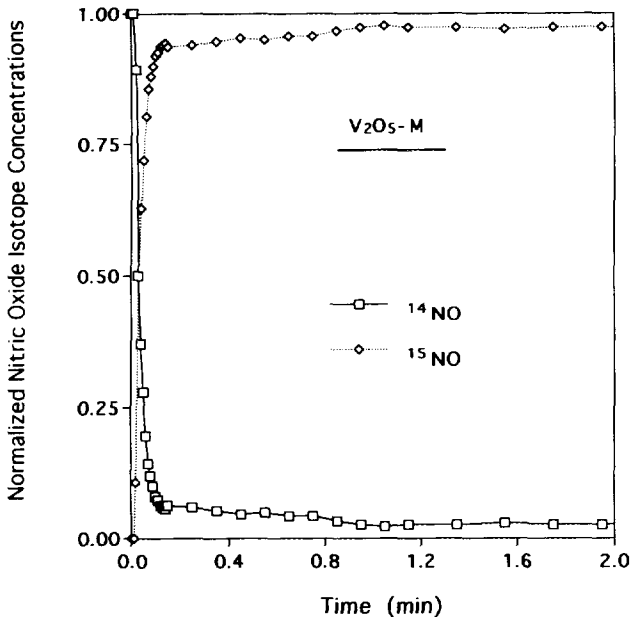

FIG. 7. Normalized nitric oxide isotope concentrations over the V_2O_5-M in $NH_3 + O_2 \rightarrow {}^{15}NH_3 + O_2$ switch.

oxide was significant over V_2O_5-M, as seen in the steady-state ammonia oxidation experiments. The ^{14}NO transient in Fig. 7 indicates a rapid relaxation, suggesting a short-lived surface species leading to NO formation. This becomes even more evident when the ^{14}NO transient is compared to the relaxation curves for unlabeled N_2O and N_2 which show a much slower decline (Figs. 8 and 9). As mentioned earlier, due to the extremely small amount of NO formed over V_2O_5-D, the detection on ^{14}NO or ^{15}NO signals was very difficult. Consequently, the nitric oxide transient curves over V_2O_5-D are not presented.

Transient curves of the nitrous oxide species over both samples are presented in Fig. 8. Although most of nitrous oxide species formed are doubly labeled, i.e., $^{15}N_2O$, resulting from two labeled ammonia molecules reacting with oxygen, a significant amount of nitrous oxide formed is, surprisingly, still unlabeled over both V_2O_5-D and V_2O_5-M for a significant period of time following the switch. The unlabeled nitrous oxide has to be formed from two unlabeled ammonia molecules, which must remain on the catalyst surface even when the gas phase has been replaced by labeled ammonia. Interestingly, there was no cross labeled nitrous oxide, i.e., $^{14}N^{15}NO$, observed over either sample.

The nitrogen transient curves shown in Fig. 9 exhibit similar trends to the nitrous oxide transients such that, although most of the nitrogen produced in the system is doubly labeled, significant amounts of the unlabeled nitrogen are present for a long period of time over both samples even after the introduction of labeled ammonia. Similar to the formation of nitrous oxide, there is no cross labeled nitrogen formation over either sample. Both N_2O and N_2 transients suggest substantially longer surface residence times, especially when compared to that of NO transient.

DISCUSSION

Catalyst Characterization

The structure of vanadium pentoxide has been studied by several researchers in the past (16, 33–35). The V_2O_5 structure is thought to be built from distorted trigonal bipyramids or distorted octahedra, sharing edges to form zigzag chains along (001) and cross-linked along (100) planes of the crystal (34). The crystals form layers parallel to the (010) plane. While the V = O sites that are located mainly on the (010) plane have been sited to have high oxidation potential (34), double- and triple-bridging oxygens and V–OH groups have also been reported as possible active sites for various reactions (16, 36, 37).

The characterization studies have explicitly shown that the two samples prepared by different thermal treatment

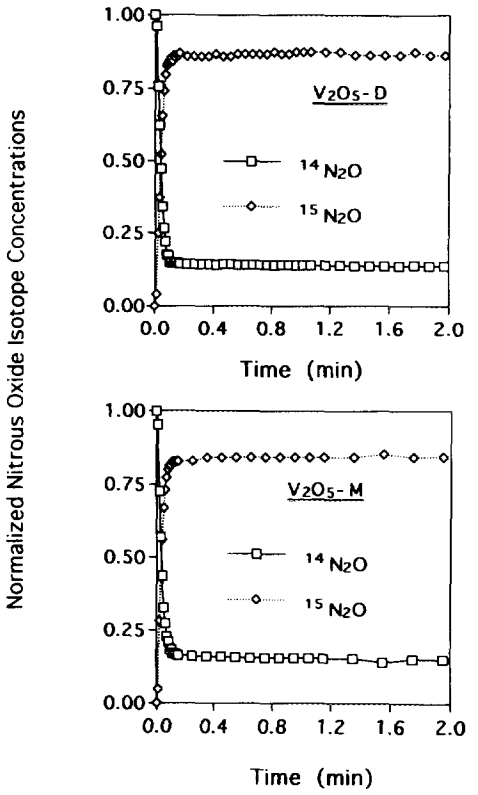

FIG. 8. Normalized nitrous oxide isotope concentrations in the $NH_3 + O_2 \rightarrow {}^{15}NH_3 + O_2$ switch.

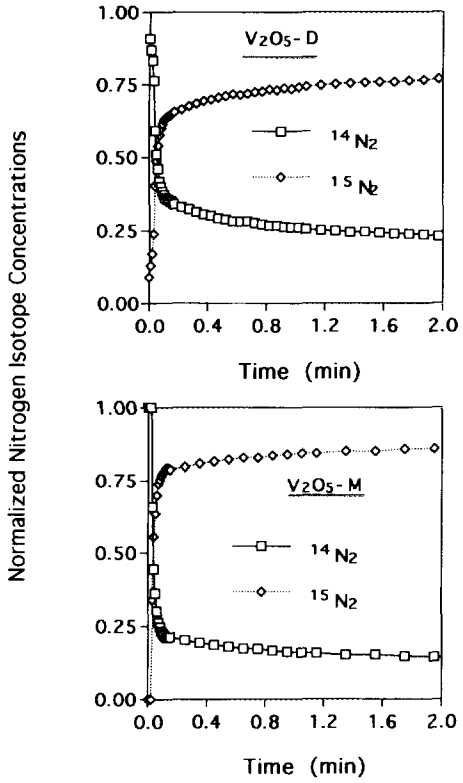

FIG. 9. Normalized nitrogen isotope concentrations in the $NH_3 + O_2 \rightarrow {}^{15}NH_3 + O_2$ switch.

techniques expose different crystal planes preferentially. While V_2O_5-M exposes mostly the (010) basal plane, V_2O_5-D exposes the side and basal planes almost in equal proportions. As a result of the preferred exposure of the (010) plane over V_2O_5-M, this sample has a higher abundance of the V = O sites as confirmed by Raman spectroscopy (band at 995 cm^{-1}). These observations are in agreement with earlier studies that have shown the V = O sites to be located on the (010) basal plane of vanadium pentoxide crystals (16, 33, 36).

Forcing and Mixing Function Measurements

The forcing function measurements were made by switching from an Ar + He mixture to a O_2 + He mixture and sending this step change through an empty reactor. The Ar decay curve represents the deviation from an ideal step function change due to any backmixing in transfer lines. Similar to the procedure outlined by Bennett and co-workers (30), the forcing function was fit using an equation of the form

$$Z_f(t) = \exp\left(\frac{t}{\tau}\right) \sum \frac{t^{(i-1)}}{(i-1)!\,\tau^{(i-1)}} \qquad [1]$$

which represents a series of n equal-volume CSTRs. Use of five CSTRs with τ values of 0.6 s gave a fit which very closely resembled the experimental forcing function. The mixing function was measured by a using a similar step change sent over the catalyst bed. The equation representing the mixing function was obtained by applying the forcing function equation to a final CSTR with the assumption that the reactor is gradientless. The mixing function equation was obtained by solving the differential equation

$$Z_f = Z + \tau_m \frac{dZ}{dt}, \qquad [2]$$

where Z_f is the normalized concentration of Ar entering the reactor and Z is the normalized concentration leaving the reactor. A value of 0.8 s for τ_m gave a good agreement with the experimental mixing curve. Figure 10 shows a comparison of the simulated forcing and mixing function curves with the experimental ones.

Oxygen Exchange Experiments

The oxygen exchange experiments performed in an empty reactor showed disappearance of the O_2 signal im-

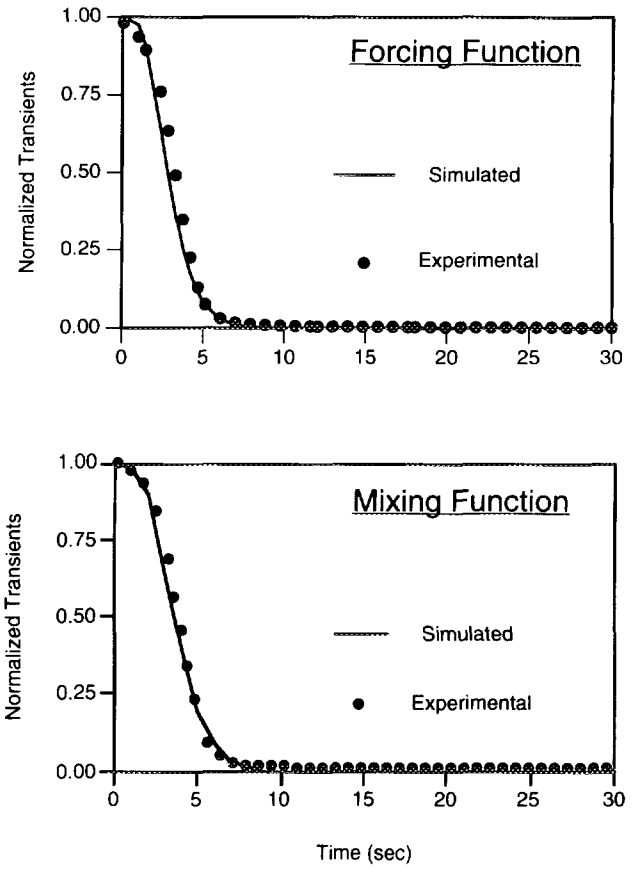

FIG. 10. Comparison of experimental and simulated curves for the forcing function and mixing function.

mediately following the switch. The area under the O_2 relaxation curve equals to that obtained in the gas-phase holdup measurement, indicating that oxygen does not interact with the reactor wall. The lack of the cross-labeled oxygen in the same experiments indicates that the homogeneous oxygen exchange under the experimental conditions does not need to be considered.

While the oxygen exchange experiments over V_2O_5-D and V_2O_5-M did not show the formation of the cross-labeled oxygen, $^{16}O^{18}O$, from the so-called scrambling process, the signal for $^{16}O_2$ reached a "pseudo-steady-state" level at a nonzero value, indicating continued exchange with the catalyst lattice. The mechanism of the exchange of gas-phase oxygen with lattice oxygen has been studied extensively by Winter (38). While the formation of the cross-labeled oxygen has been observed over some of the metal oxides (38), the absence of cross-labeled oxygen in our experiments suggests oxygen exchange taking place through the formation of a "four-atom complex" as proposed by Winter.

In agreement with what was reported in the literature (39), our experiments also suggest that the exchange of gaseous oxygen and lattice oxygen takes place on all crystal planes of V_2O_5 catalysts. However, there appears to be significant differences in the way oxygen is exchanged or abstracted over different crystal planes of the V_2O_5 crystal. The results suggest that oxygen located on the (010) plane is more readily exchangable. It exchanges with the gas phase oxygen and gets incorporated into oxygen containing products more easily. The fact that 1 min after the switch, the total rate of unlabeled oxygen incorporation into the gas phase is much higher over V_2O_5-M (1.79 μmol/m^2 · s) than it is over V_2O_5-D (0.99 μmol/m^2 · s) supports this suggestion. Further evidence of the higher activity of the surface/subsurface oxygen on the (010) plane is also found in hydrogen TPR studies which exhibit a low temperature feature over V_2O_5-M (25) as well as in oxygen exchange investigations with nitric oxide that show a more rapid oxygen exchange of NO molecules with the lattice over the same catalyst (26).

Ammonia Oxidation Experiments with Oxygen Labeling

The steady-state reaction experiments provided evidence of the structural specificity of the ammonia oxidation reaction over vanadium pentoxide crystals. The rate of ammonia conversion is much higher over V_2O_5-M than it is over V_2O_5-D. However, when the rate of ammonia conversion is normalized with respect to the basal plane area, the two catalysts were seen to have the same activity, indicating that the complete oxidation of ammonia takes place predominantly on the (010) plane. Details of the ammonia oxidation studies have been reported previously (25). Isotopic labeling studies provided additional clues as to the nature of sites that lead to ammonia oxidation. The formation rate of nitric oxide is very low over V_2O_5-D as compared to V_2O_5-M. However, it should be kept in mind that this is the observed rate and does not account for nitric oxide which is formed and gets further reacted with ammonia in an NH_3 + NO interaction.

TABLE 1

Transient Parameters for Oxygen Containing Species

	V_2O_5-M	V_2O_5-D
	Nitrous oxide[a]	
$N_{O\text{-}S}$	8.67	8.65
θ'	0.5354	0.5343
	Nitric oxide[a]	
$N_{O\text{-}S}$	19.02	—
θ'	1.1743	—
	Water[b]	
$N_{O\text{-}S}$	57.1	79.9
θ'	3.6880	5.7138

Note. $N_{O\text{-}S}$: Amount of surface/subsurface oxygen incorporated (μmol/m^2). θ': Number of monolayer equivalents.

[a] Based on basal plane area.

[b] Based on total surface area.

The amounts of surface/subsurface oxygen incorporated into various oxygen containing molecules ($N_{O\text{-}S}$) have been presented in Table 1. The values for $N_{O\text{-}S}$ are obtained by calculating the difference in the areas under the curve of each transient for the unlabeled species and the mixing function curve (Figs. 4–6) and multiplying them by the steady-state formation rate of each product. In cases where the unlabeled transient appeared to reach a pseudo-steady state, signaling a steady supply of unlabeled oxygen from the catalyst lattice, this amount was also subtracted from the total area. These values were then normalized with respect to surface area of the corresponding crystal plane over which the reaction is proposed to take place. Also presented in this table is the number of monolayer equivalents for the surface/subsurface oxygen incorporated into each product (θ').

The amount of surface/subsurface oxygen incorporated into N_2O is obtained by normalizing with respect to the area of the basal plane. The results show that, once normalized with respect to the (010) plane area, the two values are essentially equal. The number of monolayer equivalents (θ') has been calculated by dividing the number of surface/subsurface oxygen used by the number of V = O sites exposed over the basal plane. To do this, the approximation provided by Andersson (33) that gives the density of various oxygen sites on (010) and (100) planes over V_2O_5 crystals has been used. Again, the number of monolayer equivalents are essentially the same for the two catalysts, supporting our suggestion that the N_2O

production takes place exclusively on the basal plane sites.

The values for NO are also based on the basal plane area and basal plane sites. The low NO formation rates over V_2O_5-D made it difficult to obtain reliable transients for NO over this catalyst. Therefore, only the values for V_2O_5-M are presented. The number of monolayer equivalents for surface/subsurface oxygen which is larger than 1 indicates the availability of subsurface oxygen for oxygen abstraction into NO molecule.

The N_{O-S} and θ' values calculated for water are based on the overall surface area and the total number of oxygen sites exposed since it is not possible to assign all water formation to a single crystal plane. Although the formation of water as a product of the ammonia oxidation reaction would be expected to take place over the (010) plane, it is highly probable that some of the NO formed reacts further with NH_3 to form N_2 and N_2O. The catalytic job distribution, which is outlined in the following sections, suggests that the NO + NH_3 reaction leading to N_2 formation takes place predominantly over the (100) planes. Similarly, water formation from this reaction would also result from the same (100) planes. Therefore, at least some of the water formed should be normalized with respect to the area (or number of oxygen sites) of the side planes. Since we have not attempted to quantify the percent of water coming from this secondary reaction, we used the total surface area for N_{O-S} and θ' calculations for water. Therefore, the values obtained for the two catalysts are expected to be different because the extent of secondary reaction of NO over the two catalysts is most likely to be different. The fact that $N_2{}^{16}O$ signal drops to zero while the $H_2{}^{16}O$ signal remains at a non-zero value over V_2O_5-M can also be explained by the secondary reaction of NO which leads to H_2O formation over the side planes. Another important observation made from the water transients is that the pseudo-steady-state value for unlabeled water, which could taken as measure of oxygen diffusion rate from the bulk is larger over V_2O_5-D than it is over V_2O_5-M, with values of 0.34 and 0.22 μmol/m^2, respectively.

Although the surface/subsurface oxygen over the basal plane seems to be more active than the oxygen located on the side planes, the replenishment of oxygen from the catalyst bulk appears to be faster in the directions parallel to the (010) plane. This is evidenced by a higher rate of unlabeled oxygen incorporation into the gas phase in the form of oxygen containing products at "pseudo-steady-state" over V_2O_5-D than over V_2O_5-M. It appears that the rate of diffusion of oxygen parallel to the x–z plane (010) is faster than it is in the y direction. This phenomenon can possibly be explained by the layered or "sheet-like" structure of V_2O_5 parallel to the x–z plane (35), which makes the diffusion of oxygen parallel to the layers easier, providing a faster replenishment rate of the oxygen sites on the side planes by the lattice oxygen. Since the percentage of side planes exposed is larger over V_2O_5-D catalyst, the difference in the rates of incorporation of lattice oxygen to water between the two catalysts can be explained by this phenomenon. It should also be noted that the basal plane sites appear to be more readily replenished by the gaseous oxygen. However, for the side plane sites, diffusion of oxygen from the catalyst lattice seems to be a contributing factor in reoxidation of the oxygen sites, although not to the extent of the rate of reoxidation by gaseous oxygen. Similar phenomena have been reported on several metal oxides including V_2O_5 (40).

Ammonia Oxidation Experiments with Nitrogen Labeling

The ammonia oxidation reactions with labeled ammonia provided further clues regarding the adsorption characteristics of ammonia on the vanadia surfaces. After the reaction mixture was switched from [NH_3 + O_2] to [$^{15}NH_3$ + O_2], there were still significant amounts of doubly-unlabeled nitrous oxide and nitrogen ($^{14}N_2O$ and $^{14}N_2$) detected. The amount of unlabeled NO, however, was much smaller and its signal disappeared rapidly after the switch. The doubly unlabeled products could only result from the adsorbed unlabeled ammonia species which remain on the V_2O_5 surface for a considerable length of time after the gas-phase ammonia is labeled. It appears that the sites that lead to the formation of the "coupling products," i.e., nitrous oxide and nitrogen, are the same in nature since the N_2O and N_2 transients are essentially identical. However, the sites that lead to NO formation appear to be different from the ones that lead to nitrous oxide and nitrogen formation. While the ammonia species that lead to "coupling products" seem to have a longer surface residence time, the ones that are converted to NO appear to be "short-lived." An alternate explanation of the same phenomenon is that the sites that are responsible for NO formation are very active, leading to a rapid insertion of surface oxygen once the ammonia molecule adsorbs on this site. This could also support the possibility that NO formed over the basal plane could further react with ammonia over the side planes since the first step appears to take place quite rapidly.

The mean residence time (τ, s), surface coverage (θ), turn over frequency (TOF, s^{-1}), and intrinsic turn over frequency (k, s^{-1}) values obtained from the transient data are presented in Table 2. τ values are obtained by calculating the area under the transient curve and subtracting the area under the mixing function curve (τ_m). Based on the proposed reaction scheme that places direct ammonia oxidation on the basal planes, the TOF and θ values are based on the number of V = O sites on the (010) plane.

TABLE 2

Transient Parameters for Nitrogen Containing Species

	V_2O_5-M	V_2O_5-D
	Nitrous oxide	
τ (s)	15.42	13.57
k (s^{-1})	0.0644	0.0737
θ	0.2092	0.1639
TOF (s^{-1})	0.0135	0.0121
	Nitrogen	
τ (sec)	17.42	
k (s^{-1})	0.0574	29.46
θ	0.8506	0.0339
TOF (s^{-1})	0.0488	0.0287
	Nitric oxide	
τ (s)	0.1044	—
k (s^{-1})	9.5785	—
θ	0.0024	—
TOF (s^{-1})	0.0230	—

The TOF and θ values obtained for N_2O are remarkably similar for the two catalysts, supporting our suggestion that the N_2O formation through ammonia oxidation indeed takes place on the (010) plane. The TOF and θ values obtained for nitrogen are also fairly close although the agreement is not as good as it is for N_2O. The reason for this may be the formation of some of the nitrogen through the secondary reaction of NO with NH_3 over the side planes. Again, considering the larger percentage of the (100) planes over the V_2O_5-D catalyst, the values obtained for this catalyst are more likely to change if the secondary reaction could be quantified. If one considers the k values obtained for N_2O and N_2 over the V_2O_5-M catalyst, they appear to be very close to one another, indicating intrinsic turn over frequencies for the two reactions to be of the same order.

As mentioned earlier the low values obtained for the NO formation rates over V_2O_5-D made it difficult to quantify the NO transients for its catalyst. The analysis performed for V_2O_5-M was quite informative in showing a much higher k value for NO formation than those obtained for N_2 and N_2O over the same catalyst.

Control Experiments

In order to verify that the differences in the observed surface residence times of the products was indeed a catalytic phenomenon and not an art effect of the system, several control experiments were performed. In order to eliminate the possibility that ammonia could be adsorbing on the inlet lines and that the slow relaxation of unlabeled nitrogen containing species could be due to slow desorption of ammonia from the transfer lines, an experiment was designed where a switch was made from NH_3 + He mixture to an Ar + He mixture over the empty reactor. Figure 11 shows the resulting transients for ammonia and Ar. As seen in the figure, the ammonia signal declined sharply and reached zero indicating that there is no NH_3 adsorption/desorption in the transfer lines. Keeping the inlet transfer lines as short as possible and heating them continuously were the precautions taken to prevent this possibility. This result was reproduced by using $^{14}NH_3 \rightarrow {}^{15}NH_3$ switch as well. Additional experiments were performed by pulsing various mixtures of NH_3 + O_2 + He and NO + O_2 + Ar directly to the mass spectrometer to see possible delays in the signal resulting from the mass spectrometer detector. All signals were seen to have identical response times. Also performed over these catalysts were nitrogen adsorption experiments to ensure that the slow decay of unlabeled N_2 transient was not due to readsorption of the final product, but due to the longer residence time of surface species which constitutes a precursor to nitrogen. Temperature-programmed adsorption/desorption studies did not show any nitrogen adsorption on the surface under reaction conditions.

Simulation of Nitrogen-Labeled Isotope Transients

In an effort to acquire further quantitative information from the transient studies, a mathematical analysis was performed, following a procedure similar to the one outlined in the literature (29, 30, 41–44), where the unsteady-state mole balances of each unlabeled gas phase and surface species were expressed in the form of a differential equation. The model assumed three different ammonia adsorption sites, S1, S2, and S3. While S1 was assumed to be responsible for the formation of nitrogen from the

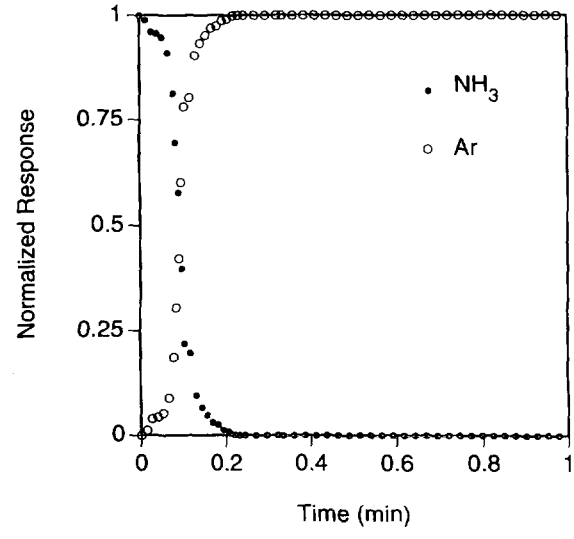

FIG. 11. Normalized NH_3 and Ar concentrations in the $NH_3 \rightarrow$ Ar switch.

interaction of NO + NH_3, S2 sites were assumed to "house" the adsorbed ammonia species which act as precursors that lead to coupling of ammonia to form N_2 and N_2O. S3 sites were assigned the role of NO formation. Based on this model, seven differential equations were written, four of them being for the normalized gas phase concentrations of unlabeled NH_3, NO, N_2, N_2O. The remaining three differential equations were written for the normalized concentrations of adsorbed ammonia species which act as precursors for the ammonia oxidation reactions giving NO (S1), N_2O + N_2 (S2), and selective reduction reaction giving N_2 (S3). The simulation equations are presented below

$$\tau_{NH_3}\left(\frac{dFNH_3(t)}{dt}\right) = Z_f(t) - FNH_3(t)(1 - X) - FNH_3(t) \quad [3]$$

$$(\beta_1 + \beta_2 + \beta_3) + \beta_1 Z_1^*(t) - X_{N_2,SCR} Z_1^*(t) + \alpha_2 Z_2^*(t)$$

$$\tau_1^*\left(\frac{dZ_1^*(t)}{dt}\right) = FNH_3(t) - Z_1^*(t)\left(\frac{\alpha_1}{\beta_1}\right) - FNO(t)\left(1 - \frac{\alpha_1}{\beta_1}\right) \quad [4]$$

$$\tau_2^*\left(\frac{dZ_2^*(t)}{dt}\right) = FNH_3(t) - Z_2^*(t)\left(1 - \frac{X_{N_2O,SCR}}{\beta_2}\right) - FNO(t)\left(\frac{X_{N_2O,SCR}}{\beta_2}\right) \quad [5]$$

$$\tau_{N_2}\left(\frac{dFN_2(t)}{dt}\right) = A\,Z_2^*(t) + (1 - A)\,FNO(t) - FN_2(t) \quad [6]$$

$$\tau_{N_2O}\left(\frac{dFN_2O(t)}{dt}\right) = E\,Z_2^*(t) + (1 - E)\,FNO(t) - FN_2O(t) \quad [7]$$

$$\tau_{NO}\left(\frac{dFNO(t)}{dt}\right) = Z_3^*(t) + FNO(t) \quad [8]$$

$$\tau_3^*\left(\frac{dZ_3^*(t)}{dt}\right) = FNH_3(t) - Z_3^*(t), \quad [9]$$

where:

X = fractional conversion of ammonia,
A = fraction of N_2 formed from NO–NH_3 interaction,
E = fraction of N_2O formed from NO–NH_3 interaction,
F_i = normalized gas-phase concentration of species i,
Z_j^* = normalized surface concentration of species j,
τ_i = gas-phase residence time for species i (s),
τ_j^* = surface residence time for species i (s),

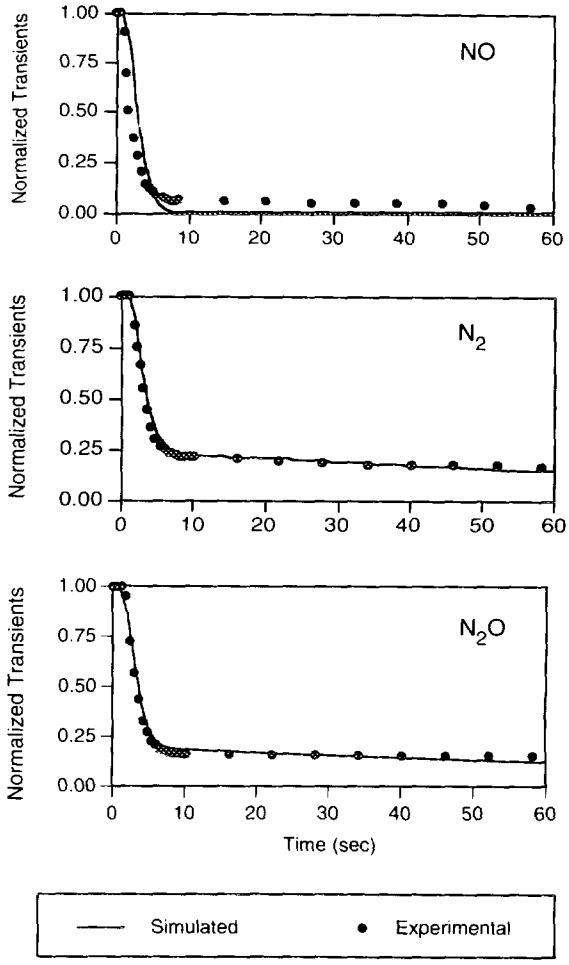

FIG. 12. Comparison of experimental and simulated transients for nitric oxide, nitrogen, and nitrous oxide.

$X_{i,SCR}$ = fractional conversion of NH_3 in NO–NH_3 reaction to produce species i,
β_j = $R_{j,ads}/R_f$,
α_j = $R_{j,des}/R_f$,
R = molar flow rate (μmols/s);

subscripts:

i = surface species adsorbed on sites 1, 2, or 3,
j = gas phase species NH_3, NO, N_2, or N_2O,
f = inlet flow.

The set of differential equations was solved simultaneously after entering values for the number of surface species for S1, S2 and S3 estimated from the experimental transients. The simultaneous solution of the seven equations was achieved numerically by using the Maple (Version 5.3) software. The results were reproduced using a FORTRAN program based on the Runge–Kutta approximation. The model predicts the normalized gas phase concentrations of the nitrogen containing species. A comparison of the simulation curves with the experimental transients for NO, N_2, and N_2O over V_2O_5-M is presented in Fig. 12. As seen in the figure, the simulation predicts

the nitrogen and nitrous oxide transients perfectly. The fit for the NO transient is also quite good, although the simulation predicts a faster decline to zero.

Some of the parameters obtained from the simulation are listed in Table 3. As expected the residence time for surface species that are acting as precursors to ammonia coupling products, i.e., N_2 and N_2O are much longer than that of the NO precursor. The model also gives a much larger k value for NO formation than the combined value for $N_2 + N_2O$, as expected. The simulation is a more realistic description of the actual system, especially when compared to a representation as a simple exponential function, since it accounts for coupled dependencies of the various surface and gas phase species. The present model can be improved significantly by quantitatively accounting for the secondary reaction of NO with ammonia. However, no such attempt is included in this article.

The model includes terms for reversible desorption of ammonia from sites S1 and S2. However, the desorption terms obtained through the best fit were negligibly small, reinforcing our experimental observation that under reaction conditions, there was no reversibly adsorbed ammonia desorbing, at any appreciable level. This result is in agreement with our earlier TPD studies (25) as well.

Catalytic Job Distribution in NH_3 Oxidation over V_2O_5 Catalysts

There have been several reports in the literature suggesting different sites for ammonia adsorption. Ammonia has been reported to adsorb as NH^{4-} species on sites adjacent to V = O bonds (13). Gasior *et al.* (16) have also suggested a similar form of adsorbed ammonia on the V-OH sites located on the side planes. The existence of $V-ONH_2$ type of species as a result of chemisorbed ammonia on the V = O sites has been suggested by Janssen *et al.* (14, 15). Kataoka and Dumesic (45) have suggested that V = O sites are responsible for the Bronsted acid character of V_2O_5 catalysts and reported ammonia adsorption on both Lewis and Bronsted acid sites on vanadia/titania (46). Topsoe (47) also reported ammonia adsorption on both Lewis and Bronsted acid sites and suggested the Bronsted acid sites or V–OH groups found on both supported and unsupported vanadia to be the principal reaction centers for NO reduction. It has also been suggested (33) that some of the oxygen is very loosely bonded to the (010) plane which can be removed at high temperatures exposing naked metal ions. These naked metal ions can possibly act as Lewis acid centers, the existence of which is suggested by several authors (34, 45, 47, 48). Although the existence of Lewis sites has been shown experimentally (47, 48) as well as theoretically (45), the extent of their involvement in the overall mechanism is believed to be negligible (33, 45).

TABLE 3

Simulation Parameters for Nitrogen Containing Surface Species

Species adsorbed on site	Precursor to:	τ_i^* (s)	k_i (s^{-1})	θ_i	TOF (s^{-1})
S1	N_2 through NO + NH_3	4.0	0.25	~1	0.25
S2	N_2, N_2O through NH_3 oxidation	90	0.011	~1	0.011
S3	NO through NH_3 oxidation	0.19	5.3	0.01	0.053

The results in this study, combined with our previous investigations (25) and the SCR investigations using isotopic tracers (26), lead us to suggest that there are at least three types of sites present on the catalyst surface for ammonia adsorption. An ammonia molecule can be thought to dissociatively adsorb on two neighboring V = O sites as follows (type A):

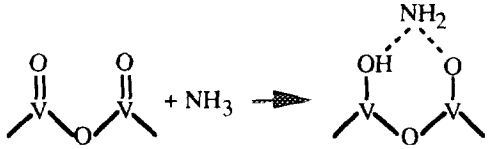

This species is thought to be short lived, but highly active, reacting, with the help of surface oxygen, to give nitric oxide and water. The nature of the species required, i.e., two neighboring V = O sites, for this type of ammonia adsorption, makes basal plane more prone to this type of reaction and since V_2O_5-M has a higher abundance of the V = O sites through increased exposure of the basal plane, this model explains the higher selectivity observed over this catalyst for NO formation in ammonia oxidation. While this reaction leads to the formation of oxygen vacancies and surface OH groups, the presence of water in the system could also lead to increased concentration of V-OH sites on the surface. In fact, similar to all oxide surfaces, the vanadia surface also is dynamic in nature under reaction conditions with V = O sites and V–OH sites interconverting to one another. It is conceivable that the V = O sites on the (010) plane neighboring V–OH sites provide the second type of ammonia adsorption sites, as shown below (type B), leading to direct oxidation of ammonia.

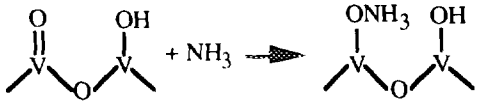

These species are thought to have a longer surface residence time and to lead to the "coupling" reaction that forms N_2 and N_2O. The absence of any cross-labeled species e.g., $^{14}N^{15}N$ or $^{14}N^{15}NO$, in the experiments involving the switch from $[NH_3 + O_2]$ to $[^{15}NH_3 + O_2]$ suggests that the two type of surface species that are formed on the basal plane do not interact with one another.

While the experimental evidence we have leads us to link ammonia oxidation with the V = O sites on the (010) plane, our related studies in SCR reactions suggest the presence of a third type of ammonia adsorption site, which is primarily located on the side planes. One possibility for this site is the hydroxyl groups which are located on the side plane and which are adjacent to other V–OH groups. The presence of these sites on the side planes of vanadium pentoxide crystals has been suggested before (16). Ammonia can be adsorbed on the V–OH sites giving the following surface species (type C):

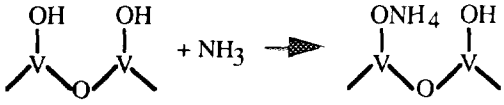

Our experimental observations (24–26) lead us to suggest that these sites play an insignificant role in direct oxidation of ammonia, but they are the active sites for selective reduction of NO. The significantly higher selectivity of the V_2O_5-D catalysts for NO reduction can be explained in terms of such a model, especially when one considers that these catalysts not only expose a larger percentage of the side plane, but are also more likely to have a large abundance of the V-OH sites due to the preparation method, which involves formation of water during the decomposition and subsequent calcination of NH_4VO_3, enhancing the concentration of hydroxyl groups on these crystal planes (37).

The isotopic labeling studies combined with our previous characterization and steady-state reaction experiments lead us to propose a reaction scheme for ammonia oxidation which involves V = O sites on the (010) planes of V_2O_5 crystals. In this scheme, ammonia can form at least two different surface species on the basal plane, depending on the immediate environment. One of the species, which is denoted as type A above is short-lived and leads to NO formation very rapidly. The other species which does not involve dissociation of NH_3 and which has a longer "surface life" leads to the coupling of ammonia, forming nitrogen and nitrous oxide. The surface oxygen vacancies created during these steps are mainly reoxidized by gas phase oxygen although it is likely that the diffusion of lattice oxygen to the surface can also contribute to the replenishment of oxygen sites, especially for the sites located on (100) planes. The ammonium ion species which are formed on the V-OH sites are thought to be the major players in selective reduction of NO. More on this subject is presented in the following publication (26).

ACKNOWLEDGMENTS

This material is based upon the work supported by the Environmental Protection Agency under Award R-815861-01-0. Partial financial support from Exxon Corporation is also gratefully acknowledged.

REFERENCES

1. Bosch, H., Janssen, F. J. J. G., van den Kerkhof, F. M. G., Oldenziel, J., van Ommen, J. G., and Ross, J. R. H., *Appl. Catal.* **25,** 239 (1986).
2. Bauerle, G. L., Wu, S. C., and Nobe, K., *Ind. Eng. Chem. Prod. Res. Dev.* **14**(4), 268 (1975).
3. Bauerle, G. L., Wu, S. C., and Nobe, K., *Ind. Eng. Chem. Prod. Res. Dev.* **17**(2), 117 (1978).
4. Morikawa, S., Yoshida, H., Takahashi, K., and Kurita, S., *Chem. Lett.* 251 (1981).
5. Nam, I-S, Eldridge, J. W., and Kittrell, J. R., *Ind. Eng. Chem. Prod. Res. Dev.* **25,** 186 (1986).
6. Haber, J., Kozlowska, A., and Kozlowski, R., *J. Catal.* **102,** 52 (1986).
7. Inomata, M., Miyamoto, A., Ui, T., Kobayashi, K., and Murakami, Y., *Ind. Eng. Chem. Prod. Res. Dev.* **21,** 424 (1982).
8. Janssen, F. J. J. G., *Kema Sci. Tech. Rep.* **6**(1), 1 (1988).
9. Kotter, M., Lintz, H.-G., Turek, T., and Trimm, D. L., *Appl. Catal.* **52,** 225 (1989).
10. Bond, G. C., and Tahir, S. F., *Appl. Catal.* **71,** 1 (1991).
11. Bosch, H. and Janssen, F., *Catal. Today* **2,** 369 (1988).
12. Takagi, M., Kawai, T., Soma, M., Onish, T., and Tamaru, K., *J. Catal.* **50,** 441 (1977).
13. Inomata, M., Miyamoto, A., and Murakami, Y., *J. Catal.* **62,** 140 (1980).
14. Janssen, F. J. J. G., van den Kerkhof, M. G., Bosch, H., and Ross, J. R. H., *J. Phys. Chem.*, **91,** 5921 (1987).
15. Janssen, F. J. J. G., van den Kerkhof, M. G., Bosch, H., and Ross, J. R. H., *J. Phys. Chem.* **91,** 6633 (1987).
16. Gasior, M., Haber, J., Machej, T., and Czeppe, T., *J. Mol. Catal.* **43,** 359 (1988).
17. Odriozola, J. A., Heinemann, H., Somorjai, G. A., Garcia de la Banda, J. F., and Pereira, P., *J. Catal.* **119,** 71 (1989).
18. Ramis, G., Busca, G., Bregani, F., and Forzatti, P., *Appl. Catal.* **64,** 259 (1990).
19. Went, G. T., Leu, L.-J., Rosin, R. R., and Bell, A. T., *J. Catal.* **134,** 492 (1992).
20. Went, G. T., Leu, L-J., and Bell, A. T., *J. Catal.* **134,** 479 (1992).
21. Went, G. T., Leu, L-J., Lombardo, S. J., and Bell, A. T., *J. Phys. Chem.* **96,** 2235 (1992).
22. Cai, Y., and Ozkan, U. S., *Int. J. Energy Environ. Econ.* **1**(3), 229 (1991).
23. Cai, Y., and Ozkan, U. S., *Appl. Catal.* **78,** 241 (1991).
24. Ozkan, U. S., Cai, Y., and Kumthekar, M. W., *Appl. Catal. A: Gen.* **96,** 365 (1993).
25. Ozkan, U. S., Cai, Y., Kumthekar, M. W., and Zhang, L., *J. Catal.* **142,** 182 (1993).
26. Ozkan, U.S., Cai, Y., and Kumthekar, M. W., *J. Catal.* **149,** 390 (1994).
27. Driscoll, S. A. and Ozkan, U. S., J. Phys. Chem. **97** (43) (1993).
28. Smith, M. R., and Ozkan, U. S., J. Catal. **142,** 226 (1993).
29. Stockwell, D. M., and Bennett, C. O., *J. Catal.* **110,** 354 (1988).
30. Stockwell, D. M., Chung, J. S., and Bennett, C. O., *J. Catal.* **112,** 135 (1988).
31. Bennett, C. O., *AIChE J.* **13**(5), 890 (1967).
32. Bennett, C. O., Cutlip, M. B., and Yang, C. C., *Chem. Eng. Sci.* **27,** 2255 (1972).
33. Andersson, A. *in* "Adsorption and Catalysis on Oxide Surfaces" (M. Che and G. C. Bond, Eds.), p. 381. Elsevier, Amsterdam, 1985.
34. Andersson, A., *J. Solid State Chem.* **42,** 263 (1982).
35. Bachmann, H. G., Ahmed, F. R., and Barnes, W. H., *Z. Kristallogr.* **115,** 119 (1961).
36. Gasior, M., and Machej, T. J., *J. Catal.* **83,** 472 (1983).

37. Miyata, H., Nakagawa, Y., Ono, T., and Kubokawa, Y., *Chem. Lett.* 1141 (1983).
38. Winter, E. R. S., *J. Chem. Soc. (A)* 2889 (1968).
39. Kera, Y., and Hirota, K., *J. Phys. Chem.* **73**(11), 3973 (1969).
40. Novakova, J., *Catal. Rev.* **4**(1), 77 (1970).
41. Happel, J., Suzuki, I., Kokayeff, P., and Fthenakis, V., *J. Catal.* **65,** 59 (1980).
42. Happel, J., Cheh, H. Y., Otarod, M., Ozawa, S., Severdia, A. J., Yoshida, T., Fthenakis, V., *J. Catal.* **75,** 314 (1982).
43. Biloen, P., Helle, J. N., van den Berg, F. G. A., and Scahtler, W. M. H., *J. Catal.* **81,** 450 (1983).
44. Zhang, X., and Biloen, P., *J. Catal.* **98,** 468 (1986).
45. Kataoka, T., and Dumesic, J. A., *J. Catal.* **112,** 66 (1988).
46. Srnak, T. Z., Dumesic, J. A., Clausen, B. S., Tornqvist, E., and Topsoe, N.-Y., *J. Catal.* **135** (1992) 246.
47. Topsoe, N.-Y., *J. Catal.* **128,** 499 (1991).
48. Belokopytov, Y. V., Kholyavenko, K. M., and Gerei, S. V., *J. Catal.* **60,** 1 (1979).